

## Cyclic testing of short-length buckling-restrained braces with detachable casings

Muhamed S. Pandikkadavath<sup>a</sup> and Dipti R. Sahoo\*

Department of Civil Engineering, Indian Institute of Technology Delhi, New Delhi-110016, India

(Received October 27, 2014, Revised December 1, 2015, Accepted January 14, 2016)

**Abstract.** Buckling-restrained braced frames (BRBFs) are commonly used as lateral force-resisting systems in the structures located in seismic-active regions. The nearly symmetric load-displacement behavior of buckling-restrained braces (BRBs) helps in dissipating the input seismic energy through metallic hysteresis. In this study, an experimental investigation has been conducted on the reduced-core length BRB (RCLBRB) specimens to evaluate their hysteretic and overall performance under gradually increased cyclic loading. Detachable casings are used for the concrete providing confinement to the steel core segments of all test specimens to facilitate the post-earthquake inspection of steel core elements. The influence of variable core clearance and the local detailing of casings on the cyclic performance of RCLBRB specimens has been studied. The RCLBRB specimen with the detachable casing system and a smaller core clearance at the end zone as compared to the central region exhibited excellent hysteretic behavior without any slip. Such RCLBRB showed balanced higher yielding deformed configuration up to a core strain of 4.2% without any premature instability. The strength-adjustment factors for the RCLBRB specimens are found to be nearly same as that of the conventional BRBs as noticed in the past studies. Simple expressions have been proposed based on the regression analysis to estimate the strength-adjustment factors and equivalent damping potential of the RCLBRB specimens.

**Keywords:** braced frames; buckling-restrained braces; component testing; energy dissipation; seismic response; yielding

---

### 1. Introduction

Buckling-restrained braces (BRBs) are the special type of axial (brace) members capable of yielding both in tension and compression (Clark *et al.* 1999). The main components of BRBs are (i) centrally placed yielding metallic core, (ii) an encasing buckling-restraining mechanism to inhibit the global buckling of the metallic core, and (iii) a de-bonding agent between the metallic core and the encasing restraint to facilitate the free expansion and contraction of the core under cyclic loading. The central core portions of these braces are commonly termed as the restrained-yielding (core) segments, which are properly guided by the restrained-unyielding (transition), and the unrestrained-unyielding (end) segments on their ends as shown in Fig. 1(a). The inelastic axial

---

\*Corresponding author, Assistant Professor, E-mail: [drsahoo@civil.iitd.ac.in](mailto:drsahoo@civil.iitd.ac.in)

<sup>a</sup>Ph.D. Student, E-mail: [msafeerpk@civil.iitd.ac.in](mailto:msafeerpk@civil.iitd.ac.in)

deformation and axial resistance of the core segment control the hysteretic response of BRBs. The restraining elements surrounding the core segments prevent their global buckling behavior, thereby, help the material to yielding in tension and compression under the reversed cyclic loading to deliver a nearly symmetric hysteretic response. Thus, BRBs are more preferred as passive seismic energy dissipation elements over the buckling-type braces (BTBs) that, otherwise, suffer from compression buckling resulting the asymmetric hysteretic response.

Extensive experimental and analytical studies have been conducted at the component level as well as the system level of buckling-restrained braced frames (BRBFs) by various researchers to investigate their seismic performance (e.g., Uang *et al.* 2004, Xie 2005). The effectiveness of debonding material between the yielding metallic steel cores and the mortar/concrete filled steel hollow sections of BRBs have also been experimentally investigated (Watanabe *et al.* 1988, Iwata *et al.* 2000, Chen *et al.* 2001). Past full-scale tests have shown the effectiveness of BRBs in resisting seismic forces in structures (Aiken *et al.* 2002, Black *et al.* 2004, Merritt *et al.* 2003, Romero *et al.* 2003, Fahnestock *et al.* 2007, Tsai and Hsiao 2008). Experimental studies on BRBs using alternative global buckling inhibition mechanisms, such as, steel mortar planks (Iwata and Murai 2006), befitting steel external tubes without mortar/concrete (Ju *et al.* 2009), steel rolled or built up sections with bolt or welded connection (Eryasar and Topyaka 2010, Chou *et al.* 2012), welded steel angles to form external tube with rotational restraints without infilled mortar/concrete (Zhao *et al.* 2011), and all steel plate weld-assembly with stiffeners and bolt connections (Wu *et al.* 2014) have shown better hysteretic response under cyclic loading.

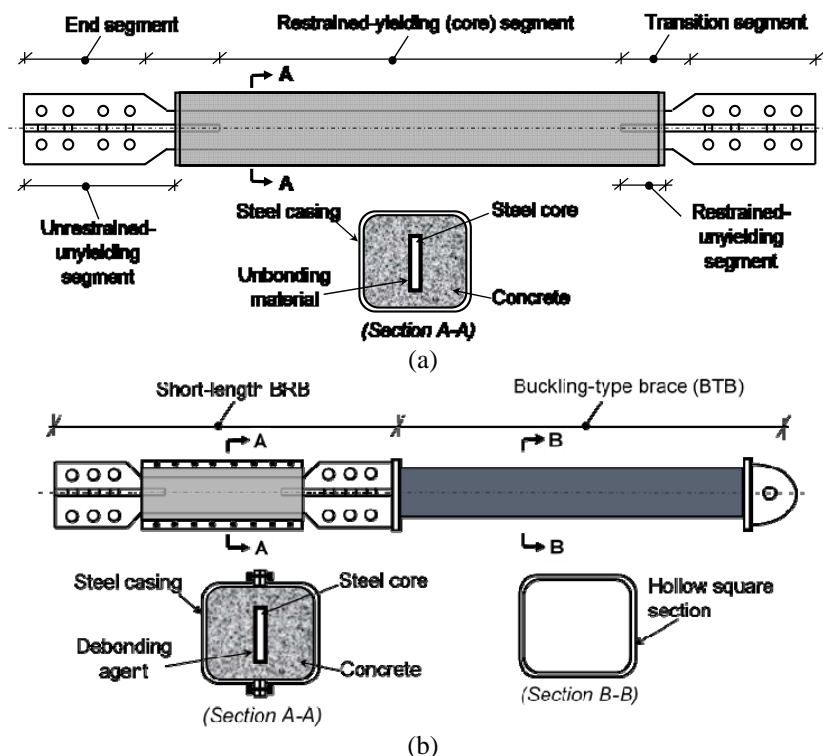


Fig. 1 Schematic representation of (a) conventional BRB and (b) hybrid brace with short-length BRB and buckling-type brace connected in series

Past studies (e.g., Sabelli *et al.* 2003, Chao *et al.* 2013) have shown that BRBFs exhibit the relatively larger post-earthquake residual drift as compared to the concentric braced frames (CBFs). The magnitude of residual drift of BRBFs largely depend on the type of beam-to-column connections in BRBFs (Ghowsi and Sahoo 2013) and the axial stiffness of BRBs. An analytical study on a medium-rise braced frame carried out by Pandikkadavath and Sahoo (2013) showed that a hybrid brace, formed by connecting BRB and BTB in series, is capable of reducing the peak residual drift response by 30%. Fig. 1(b) shows the schematic representation of a hybrid brace in which BTB portion over the dominant length of the brace is designed to remain elastic with only short BRB undergoing inelastic axial deformation under cyclic loading. The design of BRBFs requires quantification of component level strength adjustment factors for the determination of adjusted brace strengths in compression ( $P_{absC}$ ) as well as in tension ( $P_{absT}$ ). Tension strength adjustment factor ( $\omega$ ) of a BRB is a material property that relates the ultimate tensile strength to its yield strength in tension at any displacement point beyond the elastic range. Similarly, the compression strength adjustment factor ( $\beta$ ) gives the magnification of compressive yield strength with respect to the tensile yield strength in the respective inelastic deformation (due to Poisson's effect). Both values of strength adjustment factors are usually greater than unity. The yield and ultimate strengths of BRBs are computed using the following expressions

$$P_{absC} = \beta\omega P_{y_{sc}} \quad (1a)$$

$$P_{absT} = \omega P_{y_{sc}} \quad (1b)$$

$$P_{y_{sc}} = F_{y_{sc}} A_{sc} \quad (1c)$$

Where,  $P_{y_{sc}}$  is the tensile yield strength of core segment,  $F_{y_{sc}}$  is the material yield stress,  $A_{sc}$  is the cross-sectional area of steel core. ANSI/AISC-341 (2010) encourages the manufacturer of BRBs to supply the reported data of strength adjustment factors by conducting sufficient number of component and sub-assembly qualifying cyclic tests. Several experimental studies (Merritt *et al.* 2003, Newell *et al.* 2005, Benzoni and Innamorato 2007 and Kim *et al.* 2010) have been conducted on prototype BRBs to quantify these strength adjustment parameters. The conventional full-length BRBs possess 60-80% of work point to work point length as their yielding core lengths. Though the BRBs having shortened (or reduced) yielding length can increase their axial stiffness, the inelastic strain (or ductility) demand is increased on their yielding core segments. Past studies (e.g., Tremblay *et al.* 2006, Gheidi *et al.* 2011, Razavi *et al.* 2012) have been carried out on the conventional BRBs with the yielding core lengths varying between 20-50% of the work point-to-work point lengths. Since the experimental studies on the cyclic performance of short-length BRBs used as supplemental energy dissipating devices are very limited, there is a need for the further research on these BRBs in order to evaluate their energy dissipating potential, ductility, and load carrying capacity. These parameters are required for developing the design methodology for the hybrid brace as shown in Fig. 1(b).

## 2. Scope and objectives

This study is focused on the investigation of hysteretic response of short-length (or reduced-length) BRBs under cyclic loading. The main objectives of this study are to evaluate the strength-adjustment factors, energy dissipation potential, and equivalent viscous damping of reduced core-

length (RCL) BRBs by varying the core cross-section and the detailing of end connections. Usually, the core segments of BRBs are surrounded by concrete/mortar in the closed encasings. In this study, however, the detachable casings as shown in Fig. 1(b) are used to provide the restraints against the buckling of core segments of RCLBRB specimens under compressive axial loading, which facilitate the post-earthquake inspection of damaged core segments. The primary aim of this study is to compare the hysteretic performance of short-length BRBs with that of the conventional full-length BRBs. In addition, the influence of variable clearance between the steel core and confining concrete along the length of steel core on their overall cyclic performance of RCLBRB specimens has been investigated.

### 3. Experimental program

The proposed hybrid braces are intended to accrue the entire inelastic deformation within the yielding core segments of RCLBRBs during the seismic event. The RCLBRB test specimens used in this study had the yielding core lengths approximately equal to the 20% of work point-work point lengths of braces arranged in the chevron configurations in an intermediate story of a medium-rise steel building.

#### 3.1 Test specimens

Fig. 2(a) shows the various components of RCLBRB specimens. Steel core segments were inserted into the grooves left in the confining concrete with the detachable casings. These casings along with steel cores were bolted together to form the RCLBRB units. The core segments of the RCLBRB specimens consisted of central yielding portions in addition to the transition and end portions at their both ends as shown in Fig. 2(b). Two transverse end plates, as shown Fig. 2(c) were then attached to the steel core segments to facilitate the connection with the test set-up. Three test specimens with varying core cross-sections and detailing were tested in this experimental investigation. All specimens were of 600 mm long and were fabricated from steel plates of 8 mm thickness. Table 1 summarizes the dimensions of core segments of all test specimens. The length of yielding core segments of each test specimen was 300 mm, which was 50% of the total length.

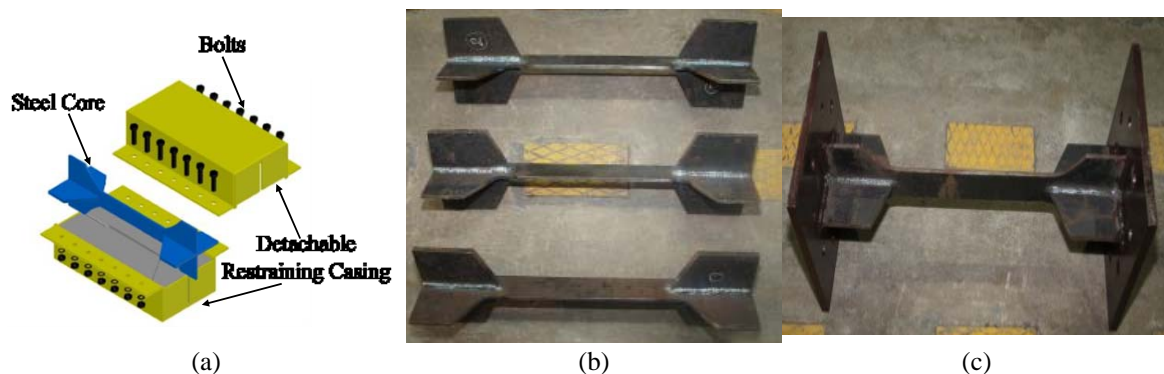


Fig. 2 Details of test specimens (a) Assembling process, (b) Fabricated steel core and (c) steel core with end plates

Fig. 3 shows the dimensions of the RCLBRB-01 specimen. The length of non-yielding restrained (i.e., transition) and non-yielding unrestrained (i.e., end) segments was 75 mm at both ends of each specimen. As expected, these segments of BRBs are dimensioned to remain elastic under the cyclic loading.

At the end zone of RCLBRB specimens, the width of plate was 200 mm. In addition, a pair of 12 mm thick steel plates of 96 mm width were provided in the transverse direction to the plane of core segment. The cross-section of the RCLBRB specimen was reduced from a cruciform section at the end to the rectangular section at the central portion by using gradually- tapered plates in the transition portion. Fig. 3 shows the dimensions and sectional views of the RCLBRB-01 specimen. The core segments of all three specimens were of exactly similar configurations except the varying cross-section area of the central yielding core segments as summarized in Table 1. The core clearance is measured in a direction normal to the plane of steel core segments as shown in Fig. 4.

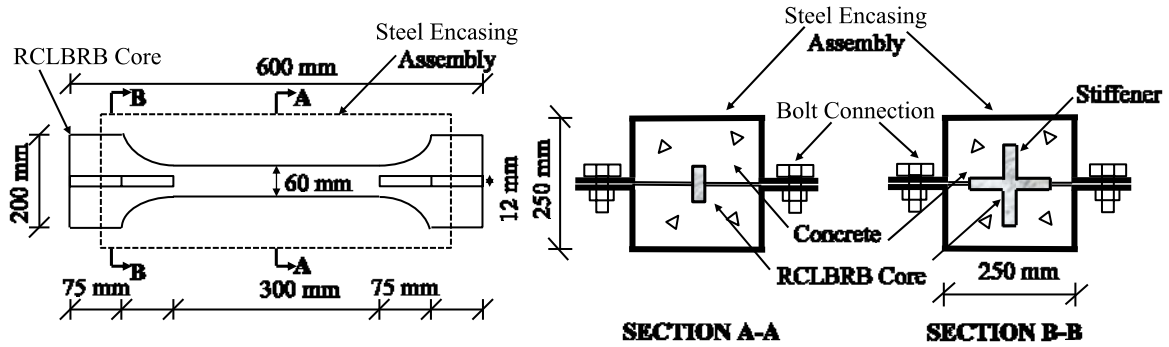


Fig. 3 Dimension details of RCLBRB-01 specimen (All dimensions are in mm)

Table 1 Details of RCLBRB core and core clearance

Specimens	Core cross-section	Central clearance	End clearance
RCLBRB-01	60 mm×8 mm	2 mm	4 mm
RCLBRB-02	55 mm×8mm	4 mm	4 mm
RCLBRB-03	52 mm×8 mm	4 mm	2 mm

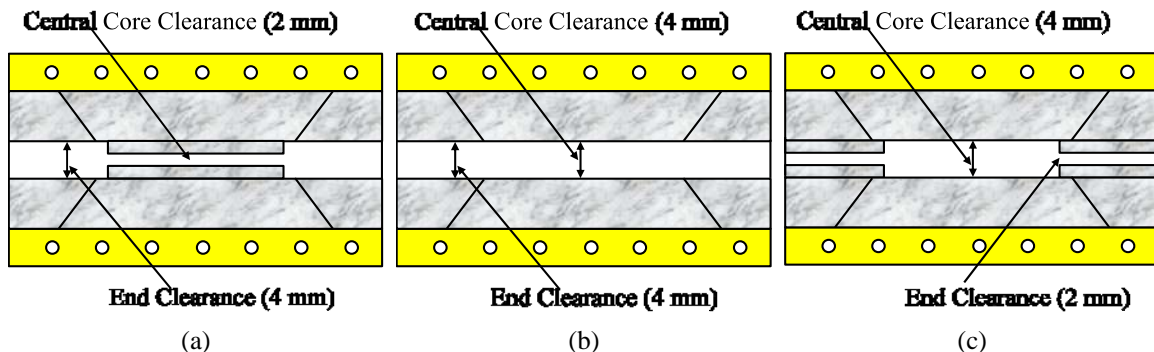


Fig. 4 Top view of detachable casing system showing core clearance (a) of RCLBRB-01, (b) RCLBRB-02 and (c) RCLBRB-03

### 3.2 Detailing of detachable casing

Concrete-filled steel casings were used for the global buckling-inhibition of the core segments of RCLBRB specimens. As stated earlier, instead of using a single hollow steel casing filled with concrete/mortar as used in case of the conventional BRBs, a pair of detachable U-shaped steel casing contained with concrete was used in the RCLBRB specimens in this study. U-shaped casings were fabricated using 6 mm thick steel plates welded together with end closing plates on both ends in the transverse direction. Outward projecting lips were provided longitudinally at the top ends of U-shaped steel casing to facilitate the attachment of two detachable units. Sufficient number of bolts were used along the projecting lips to connect these casings to form a single confining unit all around the core segments as shown in Fig. 3.

Two types of detachable casings were prepared. Encasing Type 1, as shown in Fig. 4(a), did not have transverse stiffeners on the lip plates and was used in the specimen RCLBRB-01. In case of both RCLBRB-02 and RCLBRB-03 specimens, Encasing type-2 with transverse stiffeners as shown in Fig. 4(b) was used for concrete providing restraints to the steel cores. In addition, the Encasing Type 2 was locally strengthened using two additional 8 mm diameter reinforcement bars as shown in Fig. 4(c). The fresh concrete were poured into the casings by allocating appropriate slots at the center to accommodate the steel core segments of test specimens. The slot was prepared such a way that the gap between the hardened concrete and the core was about 12 mm that leaves a 2 mm gap on each side of 8 mm thick of steel core in order to accommodate the transverse expansion of steel plate due to Poisson's effect under the axial compressive loading. An un-bonding material (grease) was used between the hardened concrete and the steel core to allow the free expansion and contraction of the steel core elements. In addition to the detachable casing, another important factor controlling the hysteretic performance of BRBs is the core clearance. The clearance between core segment at the central portion and end portion was varied for the test specimens. As shown in Table 1 and Fig. 4, three possible cases of clearance at the core and at the end of the specimen were investigated. The RCLBRB-01 specimen had the core clearance of 2 mm and the end clearance of 4 mm. The clearance values were reversed in case of the RCLBRB-03 specimen. However, the specimen RCLBRB-02 specimen had the equal clearance of 4 mm at the center as well as at the ends.

### 3.3 Test setup

Fig. 6(a) shows the assembled unit of RCLBRB specimen with end plates. One end plate was

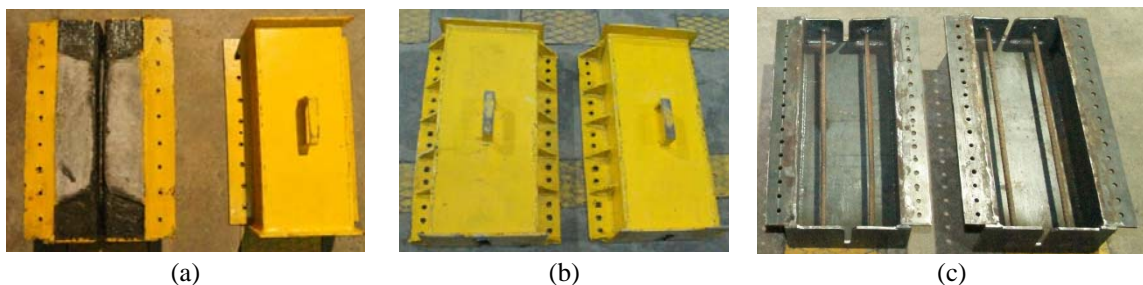


Fig. 5 Detachable casings (a) Encasing type-1 and (b) Encasing type-2, (c) Local strengthening of detachable casing

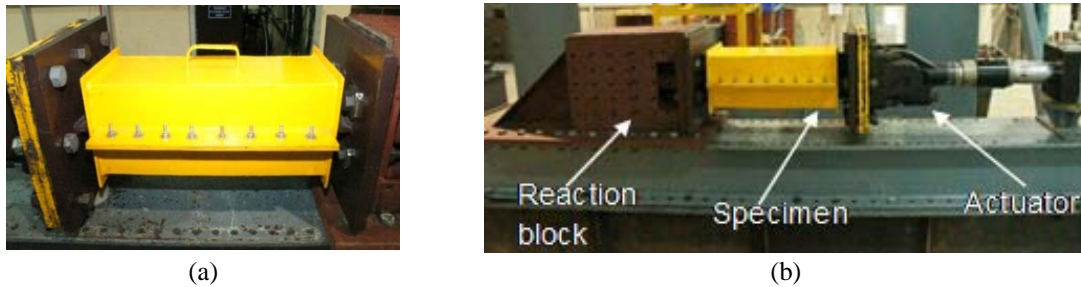


Fig. 6 (a) Assembled RCLBRB specimen and (b) Test set-up for cyclic testing

connected to a servo-controlled hydraulic actuator, whereas the other plate was connected to a reaction block as shown in Fig. 6(b). Force-rating of the actuator was 250 kN, whereas the stroke length of actuator was 250 mm. The other end of the actuator was connected to a reaction frame. The longitudinal axis of the RCLBRB component was aligned with that of the hydraulic actuator to eliminate the possible out-of-plane bending rotational demand on the test specimens. A roller support was provided just below the actuator free end to counteract the effect of its self-weight to allow the in-plane displacement of core segments of specimens. The specimens were subjected to a gradually-increased reversed-cyclic axial displacement as per the loading history. The load cell and linearly variable differential transformer (LVDT) of the servo-controlled hydraulic actuator were used to monitor the load-displacement response of the test specimens during the cyclic testing.

### 3.4 Material properties

Coupon testing of core material was carried out to determine its tensile stress-strain response using a universal testing machine (UTM) with an automatic data-acquisition system. Three coupons were tested at a loading rate of 2.5 mm/min. Figs. 7(a) and (b) shows the original and tested specimens of steel coupons. A representative stress-strain response core material is shown in Fig. 7(c). All specimens exhibited nearly similar tensile stress-strain response. The material used as core segments of RCLBRB specimens had an average yield stress of 300 MPa and an ultimate

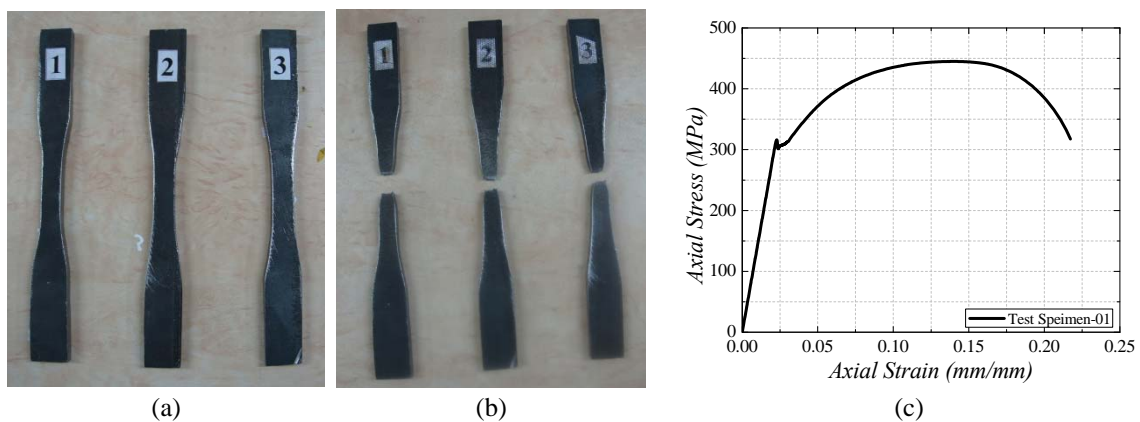


Fig. 7 Coupon test specimens (a) before testing, (b) after testing, (c) Tensile stress-strain response

stress of 443 MPa, which was nearly 1.5 times of the yield stress value. The failure (breaking) stress was 318 MPa corresponding to a strain level of 21.2%. The strain-hardening response in the stress-strain curve was noted up to 13.5% strain level.

### 3.5 Loading history

ANSI/AISC-341 (2010) specifies a standard loading protocol for the quantification testing of full-length BRBs in which the magnitude of cyclic displacement excursions were fixed depending on the values of design yield and maximum displacements based on the expected ductility demand on the full-length BRBs. However, the RCLBRB components in a hybrid bracing system as discussed earlier extends for a portion of the work point-to-work point length, which lead to the increase in the strain demand in the RCLBRB core segments. As compared to the yielding segment length of 60-80% of the total lengths of conventional full-length BRBs, RCLBRB specimens had much-smaller yielding core length (~20-30% of total length). Thus, standard loading protocol as recommended in ANSI/AISC 341-10 (2010) and FEMA-450 (2003) needs to be modified for the quantification testing of RCLBRB specimens. Fig. 8 shows the loading protocol used in the cyclic testing in this study, which was obtained by multiplying a suitable factor to the standard loading protocol amplitudes in order to achieve the similar inelastic drift displacement demands as that of the conventional full-length BRBs. The yield length of RCLBRBs were calculated initially from the geometric and material properties. The yield displacement ( $\Delta_{by}$ ) of the RCLBRB specimens was taken as 0.50 mm. The development of modified loading protocol has been developed considering the maximum strain demand in BRB that can be expected in the yielding cores of RCLBRB specimens. The targeted maximum strain in the steel core was assumed as 4%, the value achieved in the past experimental studies. The modified loading protocol, as shown in Fig. 8, consists of 6 cycles of  $\Delta_{by}$  (0.50 mm), followed by 2 cycles of  $3\Delta_{by}$  (1.5 mm), 4 cycles of  $7.5\Delta_{by}$  (3.75 mm), 4 cycles of  $15\Delta_{by}$  (7.5 mm), 2 cycles of  $20\Delta_{by}$  (10 mm) and 2 cycles of  $25\Delta_{by}$  (12.5 mm). This loading sequence achieved a maximum axial strain ( $\epsilon$ ) of 4.167 % with respect to the yielding length of the RCLBRB core segments.

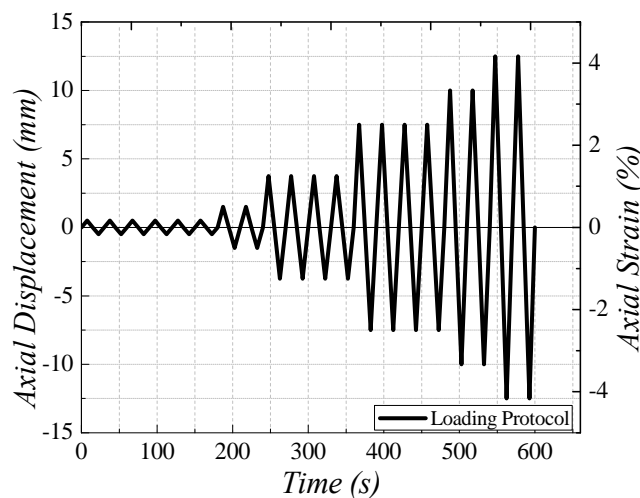


Fig. 8. Loading protocol for RCLBRB component tests

## 4. Test results

As stated earlier, test specimens were subjected to gradually-increasing reversed-cyclic displacements as per the specified loading history. The main parameters investigated are (i) overall behavior of core and casing, (ii) hysteretic behavior, (iii) strength adjustment factors, (iv) energy dissipation, and (v) equivalent viscous damping.

### 4.1 Overall behavior

As expected, all RCLBRB specimens exhibited satisfactory performance without any instability during the cyclic excursions till a core strain of 4.2%. Specimen RCLBRB-01 reached this core strain of 4.2% at the 20<sup>th</sup> cycle. In the succeeding drift cycle, the welding connection between the plates of confining casing failed making the casing unfit to provide further buckling-restraining mechanism to the yielding core as shown in Fig. 9(a). As stated earlier, the specimen RCLBRB-01 had Encasing type 1 having no intermediate stiffeners between the steel plates. The failure of welding connection resulted in the cracking of confining concrete and the localized buckling of the steel core at one of end of the specimen as shown in Fig. 9(b). Because of the reduction in the central core clearance, the higher mode buckling/yielding deformation of the core segment was noted only near the transition end of the specimen RCLBRB-01 as shown in Fig. 9(c).

Both specimens RCLBRB-02 and RCLBRB-03 were fitted with Encasing type-2 for providing buckling-restraining mechanism to the central core segments. The specimen RCLBRB-02 had a uniform slot width of 12 mm throughout the length of confining concrete leaving a core gap of 4 mm. Both specimens could able to sustain the complete drift cycles corresponding to the core strain of 4.2% without any failure of the casing. The same specimen loaded up to 5% core strain and it was observed visible pinching at higher strain rate as shown in Fig. 11(b). The hysteretic response of all specimens are shown up to the core strain of 4.2% (discussed later). At the end of the test, the confining concrete of the specimen RCLBRB-02 didn't show any major failure cracks except the local crushing at the transition zone as shown in Fig. 10(a). As compared to the specimen RCLBRB-01, the higher mode buckling deformation of the steel core of the specimen RCLBRB-02 was relatively more distributed along its length. However, instead of the expected uniformly distributed higher mode buckling, the specimen RCLBRB-02 exhibited a dominant higher mode buckling deformation near the transition zone. Finally, the specimen RCLBRB-02

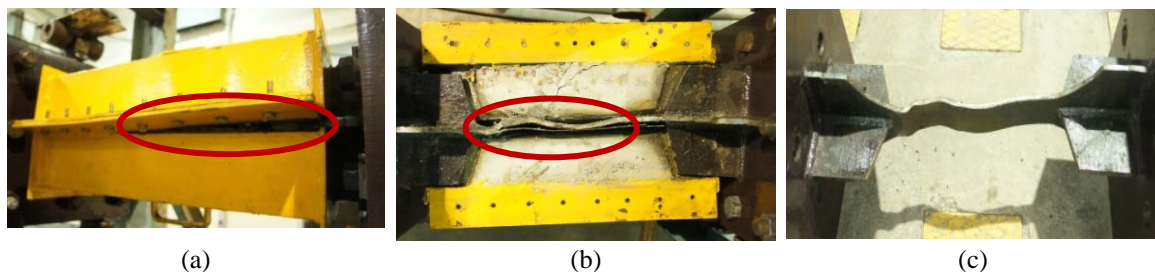


Fig. 9 State of test specimen RCLBRB-01 at 4.2% core strain level (a) Failure of welding connection of Encasing type-1, (b) Localized buckling of core segment and cracking of confining concrete, (c) Deformed shape of core segment

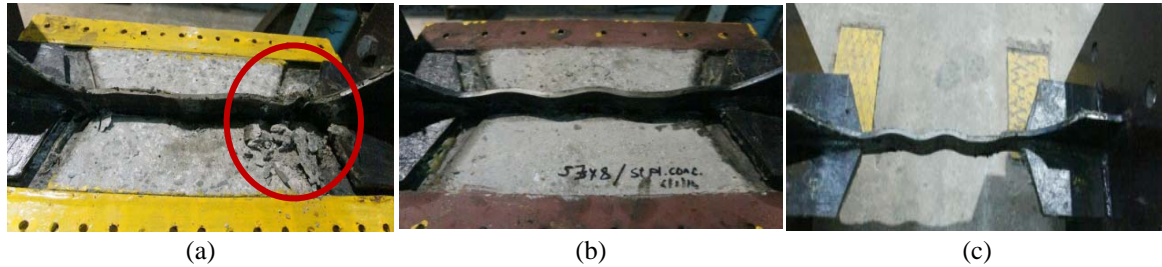


Fig. 10 (a) State of specimen RCLBRB-02 after testing showing the localized concrete crushing, (b) State of specimen RCLBRB-03 showing the undamaged concrete and deformed steel core, (c) Deformed configuration of steel core showing higher mode buckling

failed due to the fracture of steel core near the transition zone, where the maximum amplitude of compressive higher mode deformation was noticed.

From the first two RCLBRB test results, it was observed that the steel cores had a tendency to fail due to localized yielding near the transition zone. This was due to availability of equal or higher slot width at the transition zone region as compared to the central core zone. Therefore, the localized strengthening of concrete using steel reinforcement bars along with Encasing type-2 was used in the specimen RCLBRB-03 as explained earlier. In addition, the clearance between the steel core and the confining at the end segments was reduced by 50% as compared to that the central portion. As shown in Fig. 10(b), the specimen RCLBRB-03 did not show any premature failure of concrete and the casing until the core strain of 4.2% was reached. This local detailing of confining elements resulted a uniformly distributed higher mode buckling deformation of the steel core as shown in Fig. 10(c). Hence, a reduced slot width away from the yielding core length and a minimal gap (greater than at the ends) aside the RCLBRB core and the concrete cover, just to cater the Poisson effect, can improve the hysteretic response of the RCLBRBs.

#### 4.2 Hysteretic response

Axial force-displacement (hysteretic) response of RCLBRB specimens is shown in Fig. 11. All specimens reached an axial core strain of 4.2%. Specimen RCLBRB-01 exhibited two slips in the hysteretic response while maneuvering from the tension to compression inelastic cycles and vice versa as shown in Fig. 11(a). This behavior was exactly similar to that of the prototype BRB component test studies by Merritt *et al.* (2003). This slip was primarily due to the initiation of higher mode (localized) yielding deformation in compression. Minor pinching effect was also observed at the compression side of hysteretic response of the RCLBRB-01 specimen, which was due to the free out-of-plane displacement of the steel core traversing the core clearance till the concrete surface was reached under the compressive loading. Thereafter, smooth hysteretic response of the specimen was noted in the corresponding drift cycles without any discontinuity. Similar hysteretic behavior was noted for the specimen RCLBRB-02 as shown in Fig. 11(b). The asymmetric hysteretic curves at the higher drift cycles was probably due to uneven distribution of inelastic demand along the core length because of the availability of higher core clearance at the ends. As shown in Fig. 11(c), the specimen RCLBRB-03 exhibited smooth hysteretic response at all drift cycles. The slip in the hysteretic response, as noticed earlier, was completely eliminated in case of the RCLBRB-03 specimen by forcing the higher mode adjusted yielding shape in the

central region by restricting local concentration at the ends. Hence, by reducing the core clearance at the end regions away from the yielding core segments resulted in the smooth hysteretic response without any slip. It is worth mentioning that the core clearance at the central portion of the RCLBRB specimens was estimated assuming a longitudinal core strain of minimum 4% or more and a Poisson's ratio value of 0.3.

#### 4.3 Back-bone curves

Fig. 11(d) shows the comparison of backbone curves of hysteretic response of RCLBRBs. The elastic axial tension stiffness of RCLBRB test specimens were in proportion to the cross-sectional area of central core portions. The tensile axial elastic stiffness were 45.3 kN/mm, 39.6 kN/mm and 36.6 kN/mm for the RCLBRB-01, RCLBRB-02 and RCLBRB-03 specimens, respectively. The respective elastic axial stiffness in compression were 46.4 kN/mm, 44.2 kN/mm and 39.9 kN/mm. Similar trend was noticed in the post-elastic tensile stiffness of test specimens. The elastic stiffness

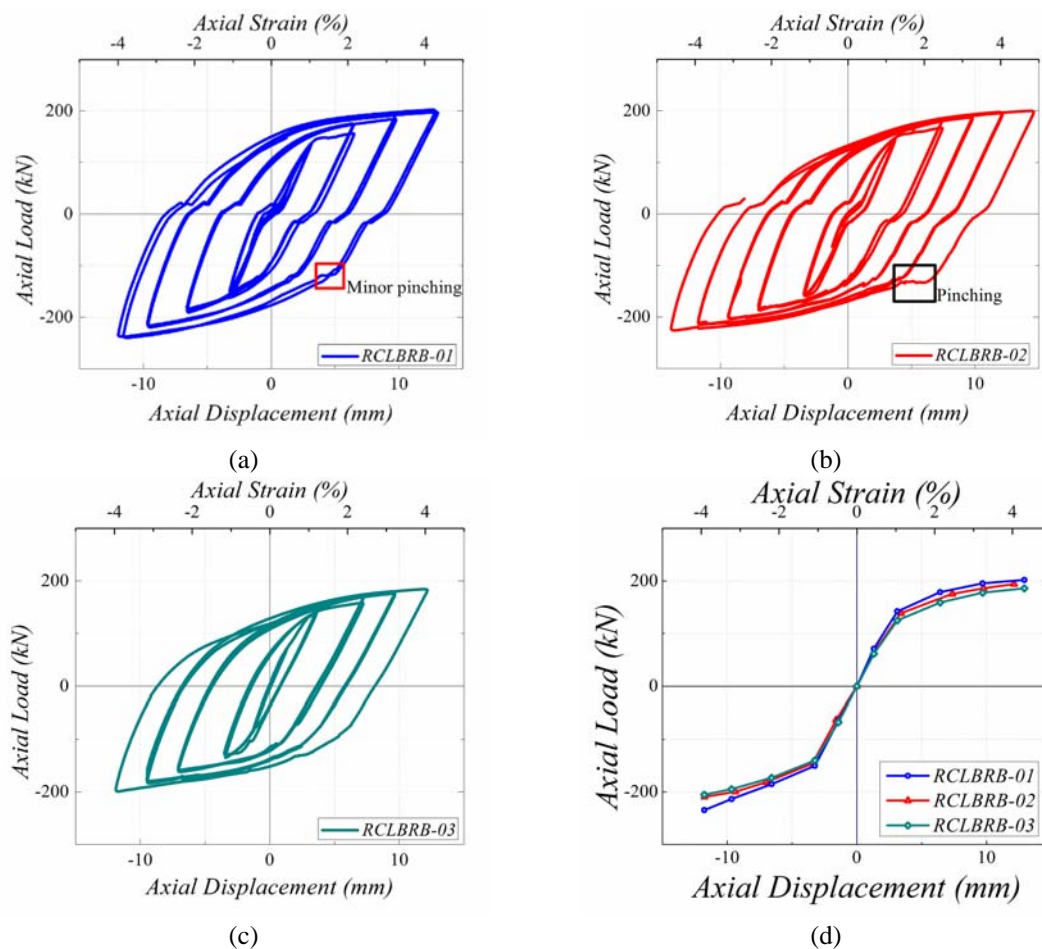


Fig. 11 Hysteretic response of (a) RCLBRB-01, (b) RCLBRB-02, (c) RCLBRB-03, and (d) Comparison of backbone curves of RCLBRBs

in the compression region of RCLBRB-03 specimen was nearly same as that of the RCLBRB-01 specimen. The post-yield stiffness of specimen RCLBRB-03 was nearly same as that of the RCLBRB-02. The average maximum tensile loads reached by the respective specimens were 202.0 kN, 194.1 kN and 180.5 kN. The average maximum compressive loads achieved by the RCLBRB-01, RCLBRB-02 and RCLBRB-03 specimens were 234.8 kN, 210.4 kN and 201.3 kN, respectively. Thus, the shape of backbone curves of the RCLBRB specimens was exactly similar to that of the conventional full-length BRBs, which can be approximately considered as bi-linear or tri-linear response for the modeling purpose.

#### 4.4 Equivalent stiffness ( $K_{eq}$ )

Equivalent axial stiffness,  $K_{eq}$  of the RCLBRB specimens at each drift cycle was computed using the following expression as per FEMA-356 (2000) provisions

$$K_{eq} = \frac{(F^+ - F^-)}{(D^+ - D^-)} \quad (1)$$

Where,  $F^+$ =the maximum tension force,  $F^-$ =the maximum compressive force,  $D^+$ =the maximum tensile displacement, and  $D^-$ =the maximum compressive displacement in each cycle. Fig. 12(a) shows the variation of the average equivalent axial stiffness with the core strain of RCLBRB specimens. The specimen RCLBRB-01 exhibited the higher equivalent stiffness at each drift (or core strain) level as compared to the other two specimens. The equivalent axial stiffness of all RCLBRB specimens was increased till the brace core strain of 1%, beyond which a gradual reduction in the stiffness was noticed with the increasing magnitude of core strain. The equivalent axial stiffness of the RCLBRBs showed a steep positive slope up to a core strain of 0.5% followed by a mild increase in the stiffness till 1% core strain. The maximum values of equivalent stiffness exhibited by the RCLBRB-01, RCLBRB-02 and RCLBRB-03 specimens were 44.2 kN/mm, 42.6 kN/mm, and 40.1 kN/mm, respectively. At an axial core strain of 4.2%, the respective values of equivalent axial stiffness were noted as 17.6 kN/mm, 16.9 kN/mm, and 15.8 kN/mm, which were about 39% of their corresponding peak values.

#### 4.5 Tension-strength adjustment factor ( $\omega$ )

Tension-strength adjustment factor ( $\omega$ ) represents the strain-hardening property of a BRB, which can be defined as the ratio of maximum tension strength,  $T_{max}$  to the tensile yield strength,  $P_{y_{sc}}$  computed as the product of core area  $A_{sc}$  and core yield stress  $F_{y_{sc}}$ . Fig. 12(b) shows the variation of  $\omega$  with the brace core strain. The average values of  $\omega$  at core strain of 4.2% strain for the RCLBRB-01, RCLBRB-02 and RCLBRB-03 specimens were found to be 1.40, 1.47 and 1.45 respectively. The best-fit line of the data points can be represented by a straight line given by the expression as follows

$$\omega = M_{\omega} \varepsilon + C_{\omega} \quad (2)$$

Where,  $M_{\omega}$  and  $C_{\omega}$  are the slope coefficients for the tension-strength adjustment factor for the RCLBRBs specimens. The values of  $M_{\omega}$  and  $C_{\omega}$  were found to be 13.25 and 0.875, respectively. The best-fit line was extrapolated beyond the recorded strain level and the tension strength adjustment factor for a core strain of 5 % was 1.54.

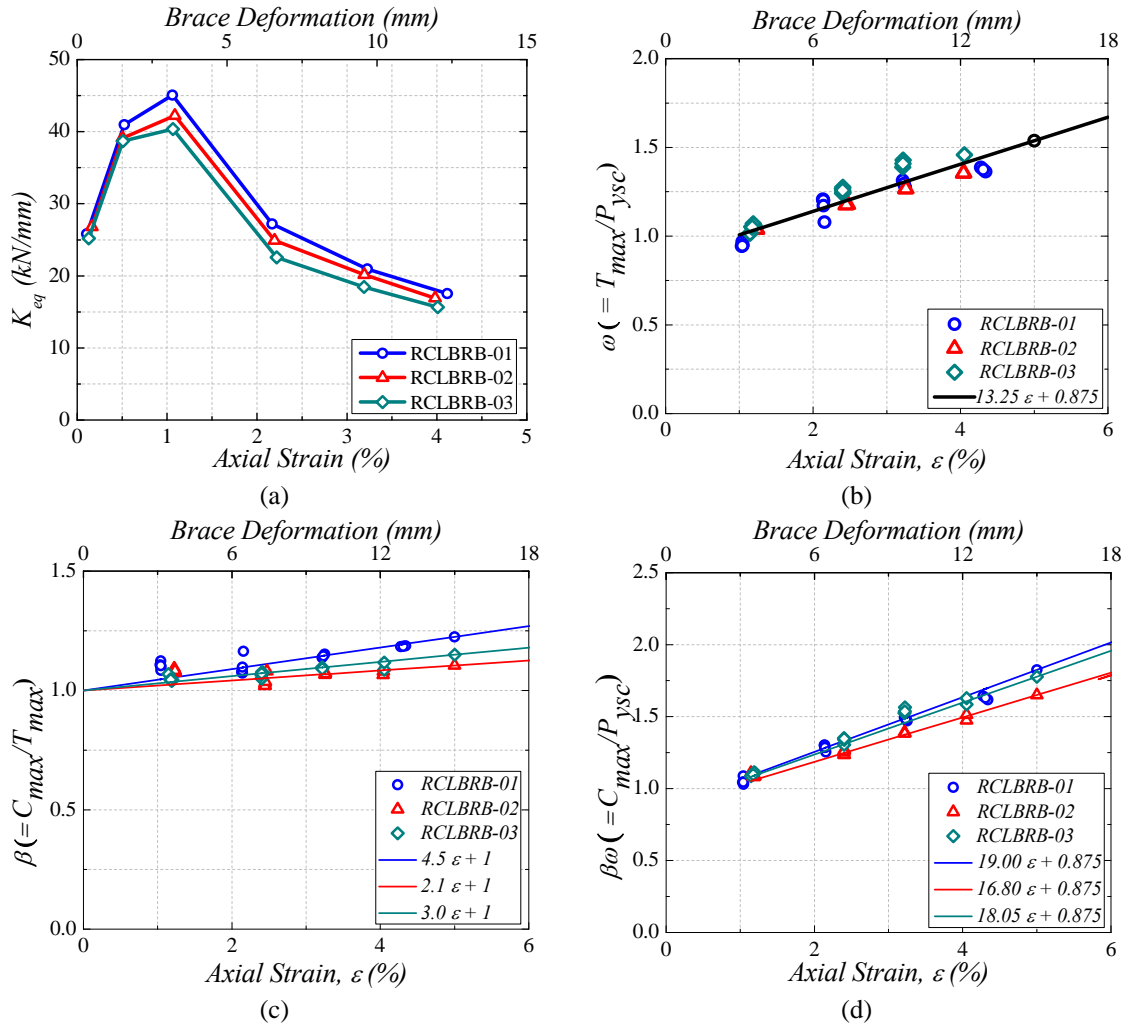


Fig. 12 (a) Variation of equivalent stiffness with core strain, (b) Tension strength adjustment factor ( $\omega$ ) comparison of RCLBRBs, (c) Compression strength adjustment factor ( $\beta$ ) comparison of RCLBRBs and (d) Comparison of  $\beta\omega$  of RCLBRBs with axial strain

#### 4.6 Compression strength-adjustment factor ( $\beta$ )

Compression strength-adjustment factor ( $\beta$ ) represents the increase of compression strength with respect to the corresponding tension strength at the same strain level and it can be defined as the ratio of maximum compressive force,  $C_{max}$  to the maximum tension force,  $T_{max}$  of the specimen. As per ANSI/AISC 341-10 (2010) provisions, the value of  $\beta$  should not be less than 1.0 for the conventional BRBs. Considering the Poisson's effect, the upper limit value of  $\beta$  was found to be 1.3 (Lai and Tsai 2001). A value higher than the upper bound value for  $\beta$  might be possible due to the friction between the steel core and the surrounding confining concrete or due to the reinsertion constraints of deformed core projections in to the casings (Daniels 2011). Fig. 12(c) shows the variation of  $\beta$  with brace core strain of the RCLBRB specimens. Depending on area of steel cross

section, availability of the higher mode yield buckling length, and confinement effectiveness, different trends were noticed in each cases. The test data's were fitted with three different straight lines having a generalized form as follows

$$\beta = M_{\beta i} \varepsilon + C_{\beta} \quad (3)$$

Where,  $M_{\beta i}$  and  $C_{\beta}$  are the slope coefficients for the respective RCLBRBs and the compression strength adjustment factor intercepts, respectively. The value of  $C_{\beta}$  was fixed to be 1.0 and the  $M_{\beta i}$  were found to be 4.5, 2.1 and 3.0 for the RCLBRB-01, RCLBRB-02 and RCLBRB-03 specimens, respectively. The  $\beta$ - $\varepsilon$  plot was extrapolated till the core strain of 5%. The average maximum value of  $\beta$  was shown by RCLBRB-01 as 1.16 and 1.20 at 4.2% and 5% core strain levels, respectively. The corresponding values for the specimen RCLBRB-02 were 1.09 and 1.11. Similarly, the values of  $\beta$  for the RCLBRB-03 specimen were 1.12 and 1.15 for the core strain of 4.2% and 5%, respectively.

#### 4.7 Total strength-adjustment factor in compression ( $\beta\omega$ )

Total strength adjustment factor in compression is defined as the product of compression-strength adjustment factor,  $\beta$  and tension strength-adjustment factor,  $\omega$ . This factor depicts the combined effect of Poisson effect and strain hardening effects of BRBs. Numerically, this gives the maximum compressive strength amplification factor with respect to the tensile yield strength of BRBs. This value governs the maximum design capacity of BRBs and the maximum considered force for the design of BRBs end connections with an appropriate factor of safety. Fig. 12(d) shows the relationship between  $\beta\omega$  and the core strain for the tested RCLBRB specimens. The same plot was fitted with suitable straight lines, which may be considered as the combined best-fit lines for the tension as well as compression strength-adjustment factors. The generalized form of the linear best-fit line can be expressed as follows

$$\beta\omega = M_{\beta\omega i} \varepsilon + C_{\omega} \quad (4)$$

The values of  $M_{\beta\omega i}$  were 19.00, 16.80 and 18.05 for the RCLBRB-01, RCLBRB-02 and RCLBRB-03 specimens, respectively. The value for  $C_{\omega}$  was same as that in the tension strength adjustment factor best-fit line. On the similar line of previous extrapolation, a value corresponding to 5% axial strain was extracted from the best-fit line. The mean value at 4.2% strain were 1.63, 1.60 and 1.62 for RCLBRB-01, RCLBRB-02 and RCLBRB-03 specimens, respectively. The respective values at a strain level of 5 % were 1.81, 1.75 and 1.79 as shown in Fig. 12(d).

#### 4.8 Hysteretic energy dissipation

The quantification of hysteretic energy dissipation potential of a BRB is an important paramter for the purpose of seismic design. As expected, the RCLBRB specimens exhibited excellent energy dissipation response. Fig. 13(a) shows the cummulative hysteretic energy potential of RCLBRB specimens per drift cycles. The cummulaitve energy dissipation response of specimens was plotted for a maximum of 20<sup>th</sup> drift cycle corresponding to 4.2% axial strain. As expected, the specimen RCLBRB-01 with the maxium cross-sectional area exhibited the highest energy dissipation in each drift cycle. The cummulative energy dissipation response of specimens varied

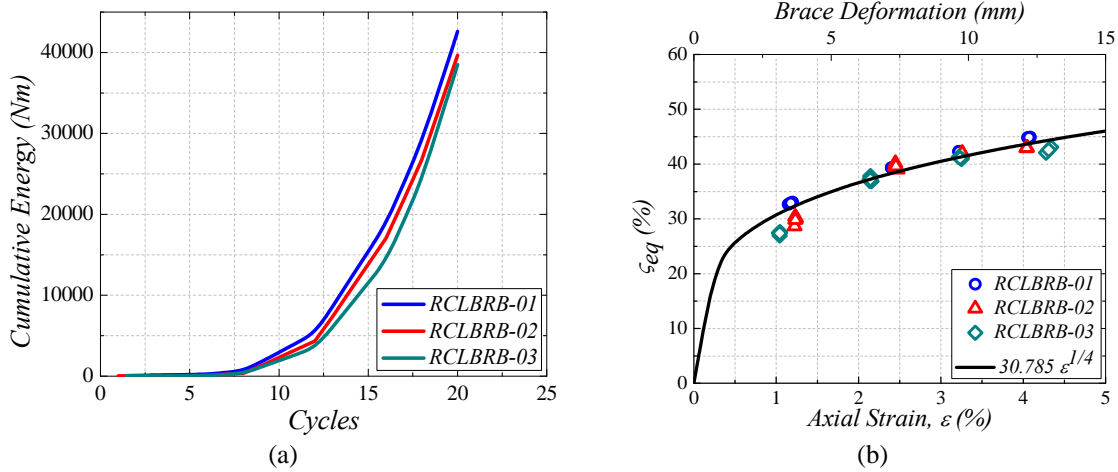


Fig. 13 (a) Cumulative energy dissipation of RCLBRBs, (b) Equivalent viscous damping of RCLBRBs

exponentially over the drift cycles. At a core strain of 4.2%, the RCLBRB-01 specimen dissipated a cumulative energy of 6825.0 kNm, whereas the specimens RCLBRB-02 and RCLBRB-03 exhibited 6425.0 kNm, 6093.8 kNm at the same core strain level, respectively.

#### 4.9 Equivalent viscous damping

The damping potential of RCLBRB specimens were computed from their corresponding hysteretic response behavior. The enclosed area under the hysteretic loop represents the energy dissipated by the specimen. The equivalent viscous energy  $\zeta_{eq}$ , of the RCLBRB specimens was computed from the hysteretic energy dissipated in each loop using FEMA-356 (2000) provision as given below

$$\zeta_{eq} = \frac{E_{loop}}{2\pi(A_T + A_C)} \quad (5)$$

Where,  $E_{loop}$  is the area dissipated in each cycle,  $A_T$  and  $A_C$  are the areas of right angled triangle at a deformation level considering origin, corresponding deformation and force of hysteresis towards tension and compression sides, respectively. Table 2 summarizes the computation of equivalent damping potential of RCLBRB specimens. The maximum value of equivalent viscous damping was 44.9% for the RCLBRB-01 specimen at a core strain of 4.2%. The corresponding values for the RCLBRB-02 and RCLBRB-03 specimens were 42.9% and 42.4%, respectively. Fig. 13(b) shows the variation of average value of equivalent viscous damping at different core strain levels. A best-fit curve was drawn to relate the equivalent viscous damping potential with the core strain and can be expressed as follows

$$\zeta_{eq} = K_{ci} \epsilon^{1/4} \quad (6)$$

$K_{ci}$  is taken as the regression constants for respective RCLBRBs. The RCLBRBs showed the equivalent viscous damping in the order of their yielding core areas. The regression co-efficients

Table 2 Computation of equivalent viscous damping per drift cycle

Specimen	Displacement		Force		Stiffness	$\beta$	$\omega$	Energy	Damping
	$D^+$ (mm)	$D^-$ (mm)	$F^+$ (kN)	$F^-$ (kN)	$K_{eq}$ (kN/mm)			$E_{loop}$ (kN/mm)	$\zeta_{eq}$ (%)
RCLBRB-01	3.3	-3.4	142.2	-156.4	44.2	1.10	0.99	1042.1	32.9
	6.4	-6.6	168.7	-183.8	27.1	1.09	1.17	2829.8	39.3
	9.7	-9.9	186.4	-212.5	20.4	1.14	1.29	5188.1	42.3
	12.9	-11.9	202.0	-234.8	17.6	1.16	1.40	7600.3	44.9
RCLBRB-02	3.6	-3.4	144.3	-155.8	42.6	1.08	1.09	987.9	29.8
	7.1	-7.0	175.7	-188.0	25.7	1.07	1.33	3118.6	38.6
	9.8	-9.4	185.7	-199.8	20.1	1.08	1.41	4856.5	42.0
	12.1	-11.8	194.1	-210.4	16.9	1.09	1.47	6510.8	42.9
RCLBRB-03	3.5	-3.5	136.0	-143.8	40.1	1.06	1.09	839.8	27.4
	7.2	-7.0	164.0	-177.5	23.9	1.08	1.31	2846.0	37.2
	9.6	-9.5	175.8	-191.6	19.2	1.09	1.41	4537.1	41.1
	12.2	-11.9	180.5	-201.1	15.8	1.12	1.45	6124.5	42.4

were found to be 31.45, 30.75 and 30.15 for the RCLBRB-01, RCLBRB-02 and RCLBRB03 specimens, respectively. The average value of the regression constant,  $K_{ci}$  was found to be 30.785.

## 5. Conclusions

Three reduced-core length BRB (RCLBRB) specimens were tested under the gradually-increased cyclic loading. Detachable casings were used in all test specimens, that can facilitate the post-earthquake inspection of core segments in the practice. The effect of local detailing of casing and confining concrete, and variable core clearance were studied. The main parameters investigated in this study were overall response, hysteretic behavior, back-bone curves, equivalent stiffness, tension-strength adjustment factor, compression-strength adjustment factor, total strength adjustment factor, hysteretic energy potential, and equivalent viscous damping.

The following conclusions can be drawn from this study:

1) RCLBRB specimen with a detachable casing system and a reduced core clearance at the end zone as compared to the central region exhibited the excellent the hysteretic behavior without any slip and balanced higher mode yielding deformation up to an axial strain level of 4.2% without any premature instability.

2) The maximum values of tension-strength adjustment factor were 1.45 and 1.54 for the RCLBRB-03 specimen at core strain level of 4.2% and 5.0%, respectively. The compression-adjustment factors for the RCLBRB specimens were nearly 1.15. Thus, the strength-adjustment factors for the RCLBRB specimens were nearly same as that of the conventional BRBs as noticed in the past studies.

3) All RCLBRB specimens showed excellent energy dissipation and damping potential. The average value of equivalent viscous damping was found to be 43.5% at a core strain level of 4.2%. In addition, simple expressions have been proposed based on the regression analysis to estimate the strength-adjustment factors and equivalent damping potential of the RCLBRB specimens.

4) The results of these component studies are extremely important for the design of combined bracing system. However, further sub-assembly studies are required to assess the cyclic performance of the combining bracing system and to identify the critical design parameters for ensuring its in-plane behavior.

## Acknowledgements

The financial support by Board of Research in Nuclear Sciences (BRNS), Department of Atomic Energy, India in conducting this research is greatly acknowledged. The help and support extended by the Structural Engineering Laboratory staff in the experimental work is highly appreciated.

## References

- Aiken, I.D., Mahin, S.A. and Uriz, P.R. (2002), "Large-scale testing of buckling-restrained braced frames", *Proceedings of the Japan Passive Control Symp.*, Tokyo Institute of Technology, Japan.
- ANSI/AISC 341-10 (2010), *Seismic provisions for structural steel buildings*, American Institute of Steel Construction, Chicago, IL.
- Benzoni, G. and Innamorato, D. (2007), *Star Seismic brace tests mercy San Juan hospital project*, Report No. SRMD- 2007/05-rev2, University of California, San Diego, CA.
- Black, C.J., Makris, N. and Aiken, I.D. (2004), "Component testing, seismic evaluation and characterization of buckling-restrained braces", *J. Struct. Eng.*, ASCE, **130**(6), 880-894.
- Chao, S.H., Karki, N.B. and Sahoo, D.R. (2013), "Seismic behavior of steel buildings with hybrid braced frames", *J. Struct. Eng.*, ASCE, **139**(6), 1019-1032.
- Chen, C.C., Chen, S.Y. and Liaw, J.J. (2001), "Application of low yield strength steel on controlled plastification ductile concentrically braced frames", *Can. J. Civ. Eng.*, **28**(5), 823-836.
- Chou, C.C., Liu, J.H. and Pham, D.H. (2012), "Steel buckling-restrained braced frames with single and dual corner gusset connections: seismic tests and analyses", *Earthq. Eng. Struct. Dyn.*, **41**(7), 1137-1156.
- Clark, P., Aiken, I., Kasai, K., Ko, E. and Kimura, I. (1999), "Design procedures for buildings incorporating hysteretic damping devices", *Proceedings of 1999 Annual Convention of the Structural Engineers Association of California (SEAOC)*, Santa Barbara, California.
- Daniels, M. (2011), "Towards characteristic over strength curves for buckling- restrained braces", *Proceedings of 2011 Annual Convention of the Structural Engineers Association of California*, Santa Barbara, California.
- Eryasar, M.J. and Topkaya, C. (2010), "An experimental study on steel-encased buckling-restrained brace hysteretic dampers", *Earthq. Eng. Struct. Dyn.*, **39**(5), 561-581.
- Fahnestock, L.A., Sause, R. and Ricles, J.M. (2007), "Seismic response and performance of buckling-restrained braced frames", *J. Struct. Eng.*, ASCE, **133**(9), 1195-1204.
- FEMA-450 (2003), *NEHRP Recommended Provisions for Seismic Regulations for New buildings and Other Structures*, Part 1- Provisions, Federal Emergency Management Agency, Washington, DC.
- FEMA 356 (2000), *Prestandard and Commentary for the Seismic Rehabilitation of Buildings*, Federal Emergency Management Agency, Washington, DC.
- Gheidi, A., Mirtaheeri, M., Zandi, A.P. and Alanjari, P. (2011), "Effect of filler material on local and global behaviour of buckling-restrained braces", *Struct. Des. Tall Spec. Build.*, **20**(6), 700-710.
- Ghowsi, A.F. and Sahoo, D.R. (2013), "Seismic performance of buckling-restrained braced frames with varying beam-column connections," *Int. J. Steel Struct.*, **13**(4), 607-621.
- Iwata, M. and Murai, M. (2006), "Buckling-restrained brace using steel mortar planks: Performance

- evaluation as a hysteretic damper”, *Earthq. Eng. Struct. Dyn.*, **35**(14), 1807-1826.
- Iwata, M., Kato, T. and Wada, A. (2003), “Performance evaluation of buckling-restrained braces in damage-controlled structures: Behavior of steel structures in seismic area”, *Proceedings of the 4th International Conference, Behavior of steel structures in seismic areas (STESSA)*, Naples, Italy.
- Ju, Y.K., Kim, M.H., Kim, J. and Kim, S.D. (2009), “Component tests of buckling-restrained braces with unconstrained length”, *Eng. Struct.*, **31**(2), 507-516.
- Kim, D.W., Sim, H.B., Uang, C.M. and Benzoni, G. (2010), *Subassemblage testing of core-brace buckling-restrained braces (H Series)*, Report No. TR-09/01, University of California, San Diego, CA.
- Lai, J.W. and Tsai, K.C. (2001), *A study of buckling-restrained braced frames*, Report No. CEER/R90-07, Center for Earthquake Engineering Research, National Taiwan University, Taiwan. (in Chinese)
- Merritt, S., Uang, C.M. and Benzoni, G. (2003), *Subassemblage testing of core brace buckling-restrained braces*, Report No. TR-2003/01, Dept. of Struct. Eng., University of California at San Diego, USA.
- Newell, J., Uang, C.M. and Benzoni, G. (2005), *Subassemblage testing of core-brace buckling-restrained braces (F Series)*, Report No. TR-05/01, University of California, San Diego, CA.
- Pandikkadavath, M.S. and Sahoo, D.R. (2013), “Seismic performance of steel frame structures with hybrid concentrically brace systems”, *Proceedings of the International Conference on rehabilitation and restoration of structures*, Chennai, India.
- Razavi, S.A., Mirghaderi, S.R., Hosseini, A. and Shemshadian, M.E. (2012), “Reduced length buckling restrained brace with steel plates as restraining segment”, *Proceedings of the 13<sup>th</sup> World Conference Earthquakes Engineering*, Lisboa.
- Romero, P., Revelry, L., Miller, P. and Okahashi, T. (2003), *Full-scale testing of WC Series buckling-restrained braces*, Dept. of Civil and Env. Eng., University of Utah, USA.
- Sabelli, R., Mahin, S.A. and Chang, C. (2003), “Seismic demands on steel braced frame buildings with buckling-restrained braces”, *Eng. Struct.*, **25**(5), 655-666.
- Tremblay, R., Bolduc, P., Neville, R. and Devall, R. (2006), “Seismic testing and performance of buckling-restrained bracing systems”, *Can. J. Civ. Eng.*, **33**(2), 183-198.
- Tsai, K.C. and Hsiao, P.C. (2008), “Pseudo-dynamic test of a full-scale CFT/BRB frame-part II: Seismic performance of buckling-restrained braces and connection”, *Earthq. Eng. Struct. Dyn.*, **37**(7), 1099-1115.
- Uang, C.M., Nakashima, M. and Tsai, K.C. (2004), “Research and application of buckling-restrained braced frames”, *Int. J. Steel Struct.*, **4**(4), 301-313.
- Watanabe, A., Hitomi, Y., Saeki, E., Wada, A. and Fujimoto, M. (1988), “Properties of brace encased in buckling-restrained concrete and steel tube”, *Proceedings of the 9th World Conf. on Earth. Eng.*, Tokyo, Japan.
- Wu, A.C., Lin, P.C. and Tsai, K.C. (2014), “High-mode buckling responses of buckling restrained brace core plates”, *Earthq. Eng. Struct. Dyn.*, **43**(3), 375-393.
- Xie, Q. (2005), “State of the art buckling-restrained braces in Asia”, *J. Const. Steel Res.*, **61**(6), 727-748.
- Zhao, J., Wu, B. and Ou, J. (2011), “A novel type of angle steel buckling-restrained brace: Cyclic behavior and failure mechanism”, *Earthq. Eng. Struct. Dyn.*, **40**(10), 1083-1102.